

Supplementary Material

MOFs-derived carbon coated Cu₃P with Ni doping as advanced supercapacitor electrode materials

Xuan He^a, Yuhong Jin^{b*}, Miao Jia^c, Mengqiu Jia^{a*}, Hao Wang^b, Muhammad Imran^d

^aBeijing Key Laboratory of Electrochemical Process and Technology for Materials,
Beijing University of Chemical Technology, Beijing 100029, China

^bKey Laboratory for New Functional Materials of Ministry of Education, Institution of
Advanced Energy Materials and Devices, Faculty of Materials and Manufacturing,
Beijing University of Technology, Beijing 100124, PR China

^cCollege of Chemistry and Materials Engineering, Beijing Technology and Business
University, Beijing 100048, P. R. China.

^dDepartment of Chemistry, Faculty of Science, King Khalid University, PO Box 9004,
Abha, 61413, Saudi Arabia

Fig. S1. XRD patterns of Cu-MOF.

Fig. S2. XRD patterns of Cu@C.

Fig. S3. XRD of Cu₃P/C-5%Ni, Cu₃P/C-10%Ni and Cu₃P/C-15%Ni.

Fig. S4. SEM image of Cu₃P/C-6%Ni at high magnification.

Fig. S5. SEM images of (a) Cu-MOF-3%Ni; (b) Cu-MOF-4%Ni; (c) Cu-MOF-5%Ni; (d) Cu-MOF-6%Ni; (e) Cu-MOF-10%Ni; (f) Cu-MOF-15%Ni.

Fig. S6. SEM images of (a) Cu/C; (b) Cu/C-3%Ni; (c) Cu/C-4%Ni; (d) Cu/C-5%Ni; (e) Cu/C-6%Ni; (f) Cu/C-10%Ni; (g) Cu/C-15%Ni.

Fig. S7. SEM images of (a) Cu₃P/C-3%Ni; (b) Cu₃P/C-4%Ni; (c) Cu₃P/C-5%Ni; (d) Cu₃P/C-10%Ni; (e) Cu₃P/C-15%Ni.

Fig. S8. SEM images of the product by direct phosphorization of Cu-MOF.

Fig. S9. EDS mapping of Cu, P, N and C elements for Cu₃P/C.

Fig. S10. CV curves of (a) Cu₃P/C; (b) Cu₃P/C-3%Ni; (c) Cu₃P/C-4%Ni; (d) Cu₃P/C-5%Ni; (e) Cu₃P/C-10%Ni and (f) Cu₃P/C-15%Ni electrode at different scan rates.

Table S1. Specific capacitances of the Cu₃P-based electrodes at different scan rates.

Fig. S11. GCD curves of (a) Cu₃P/C; (b) Cu₃P/C-3%Ni; (c) Cu₃P/C-4%Ni; (d) Cu₃P/C-5%Ni; (e) Cu₃P/C-10%Ni and (f) Cu₃P/C-15%Ni electrode at different current densities.

Table S2. Specific discharge capacitance of Cu₃P-based electrodes.

Fig. S12. EIS plots of Cu₃P-based-samples.

Fig. S13. EIS plots of initial and after 10000 cycles, inset shows the equivalent circuit and enlarged section.

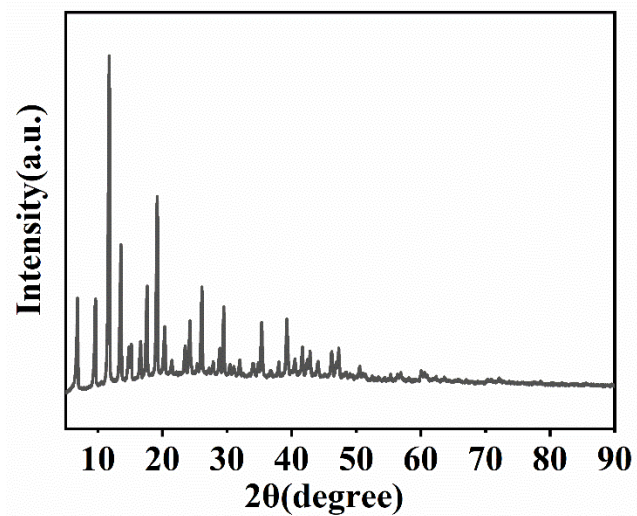


Fig. S1. XRD patterns of Cu-MOF.

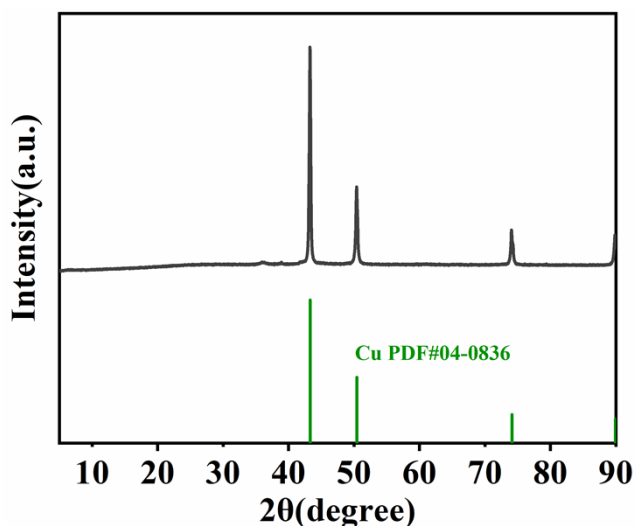


Fig. S2. XRD patterns of Cu@C.

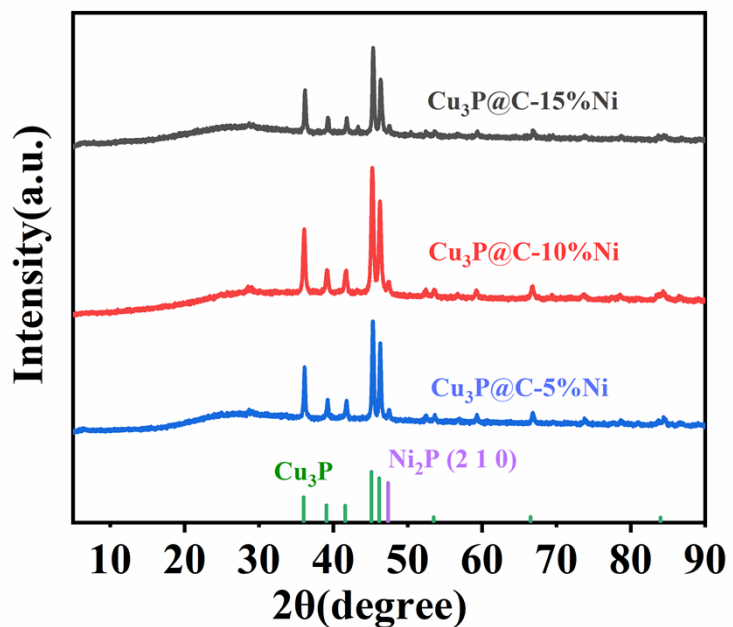


Fig. S3. XRD of Cu₃P/C-5%Ni, Cu₃P/C-10%Ni and Cu₃P/C-15%Ni

The samples doped with Ni show the diffraction peak of Ni₂P corresponding to the crystal plane.

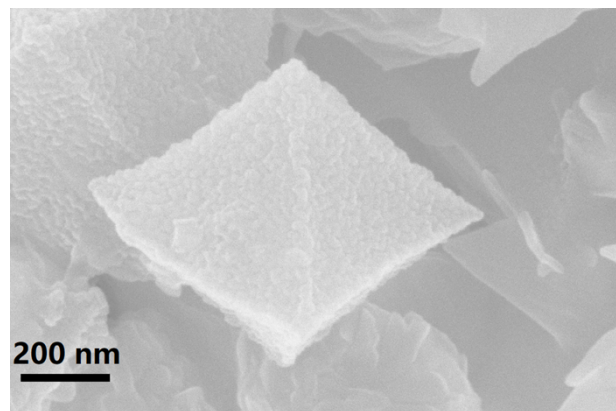


Fig. S4. SEM image of Cu₃P/C-6%Ni at high magnification.

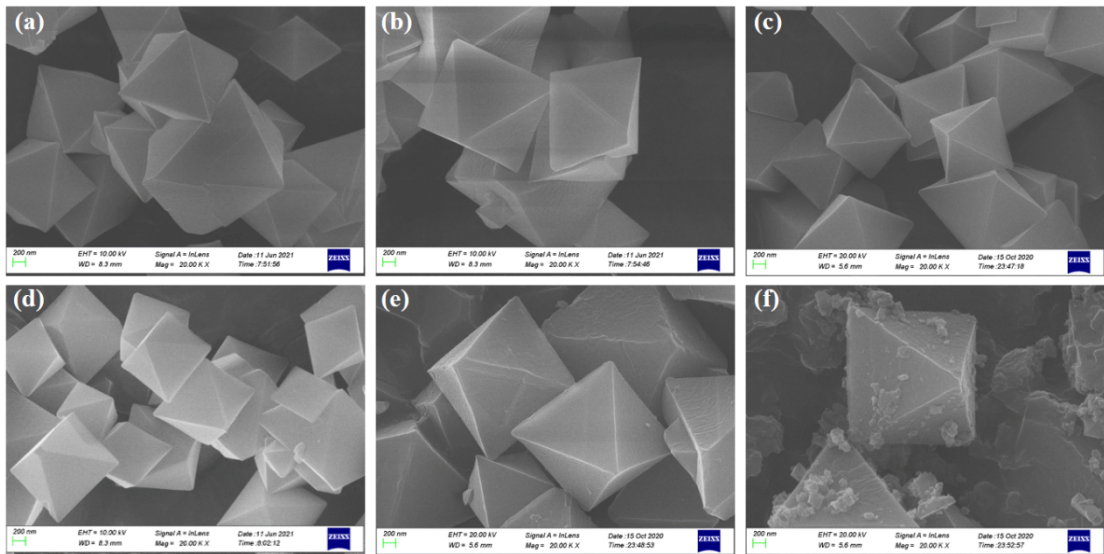


Fig. S5. SEM images of (a) Cu-MOF-3%Ni; (b) Cu-MOF-4%Ni; (c) Cu-MOF-5%Ni; (d) Cu-MOF-6%Ni; (e) Cu-MOF-10%Ni; (f) Cu-MOF-15%Ni.

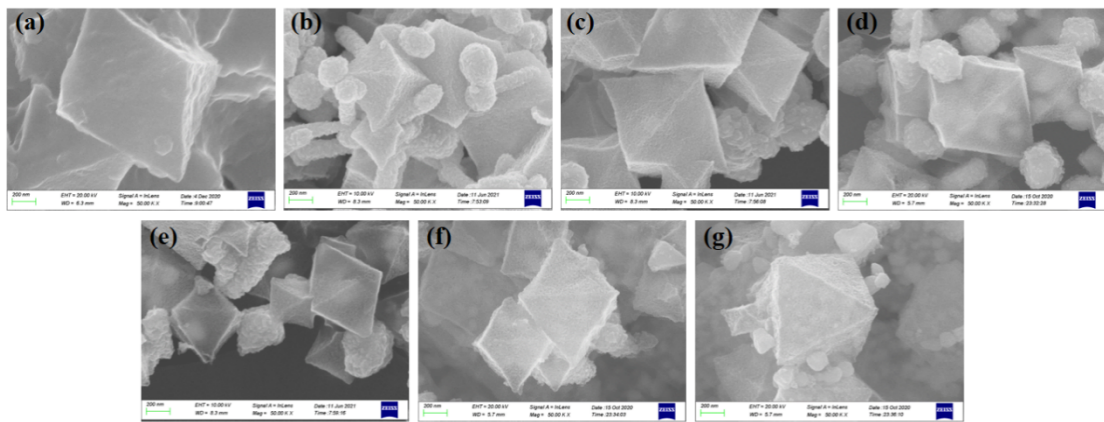


Fig. S6. SEM images of (a) Cu/C; (b) Cu₃P/C-3% Ni; (c) Cu₃P/C-4% Ni; (d) Cu₃P/C-5% Ni; (e) Cu₃P/C-6% Ni; (f) Cu₃P/C-10% Ni; (g) Cu₃P/C-15% Ni.

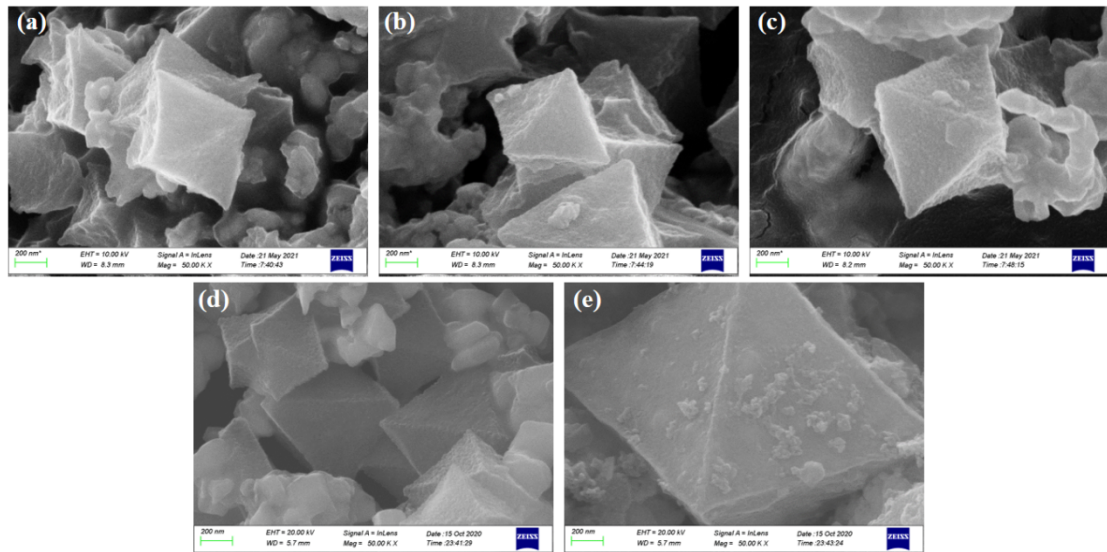


Fig. S7. SEM images of (a) Cu₃P/C-3% Ni; (b) Cu₃P/C-4% Ni; (c) Cu₃P/C-5% Ni; (d) Cu₃P/C-10%Ni; (e) Cu₃P/C-15%Ni.

The Cu-MOF-based precursors all showed smooth surfaces, while nanoparticles gathered on the surfaces after carbonization and phosphorization.

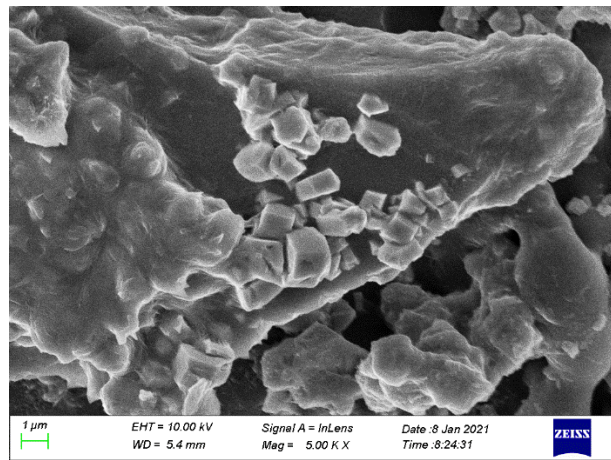


Fig. S8. SEM images of the product by direct phosphorization of Cu-MOF.

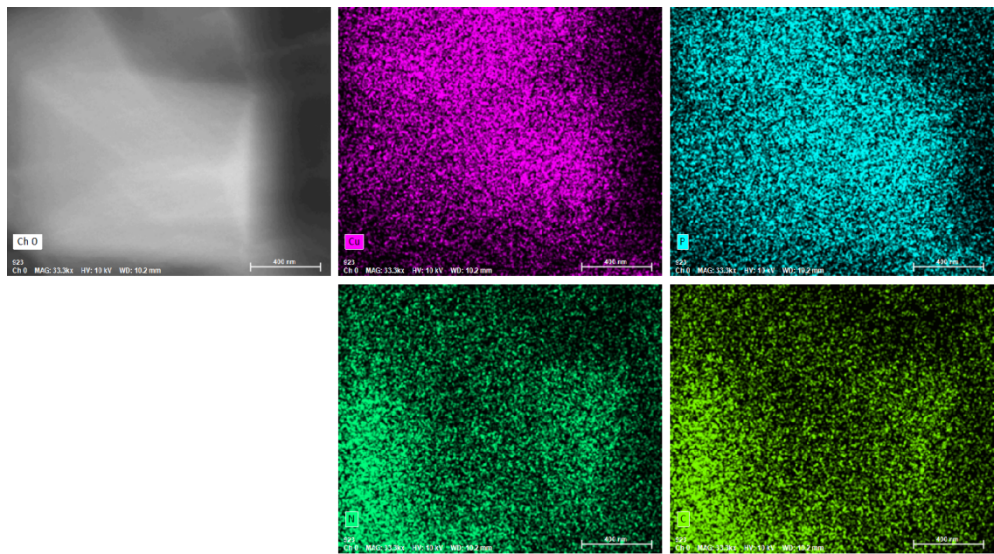


Fig. S9. EDS mapping of Cu, P, N and C elements for Cu₃P/C.

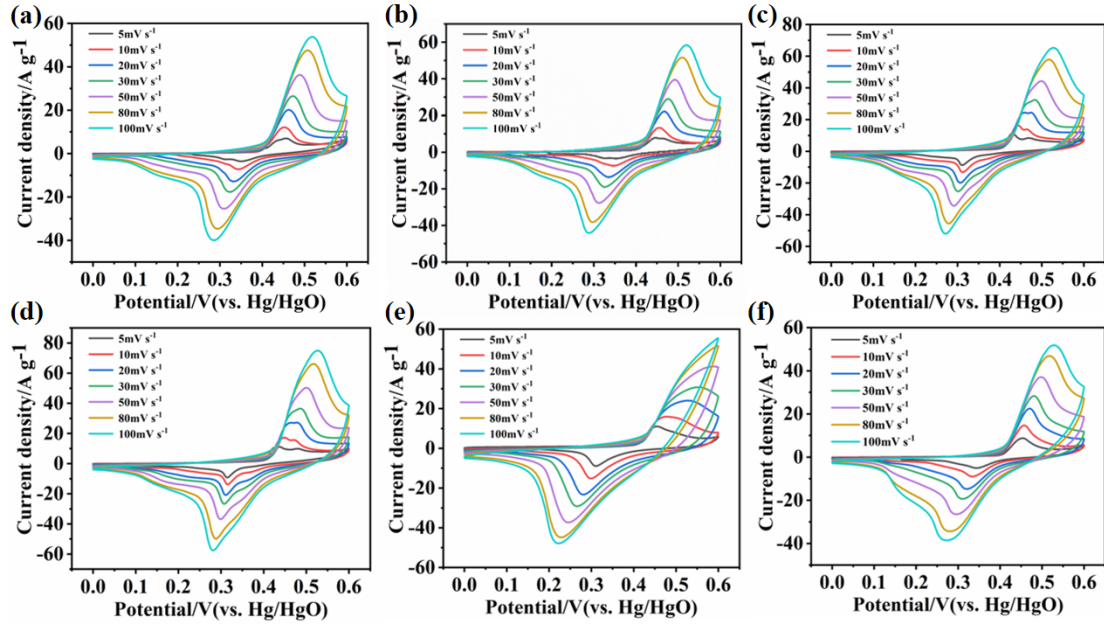


Fig. S10. CV curves of (a) $\text{Cu}_3\text{P}/\text{C}$; (b) $\text{Cu}_3\text{P}/\text{C}-3\%$ Ni; (c) $\text{Cu}_3\text{P}/\text{C}-4\%$; (d) $\text{Cu}_3\text{P}/\text{C}-5\%$; (e) $\text{Cu}_3\text{P}/\text{C}-10\%$ and (f) $\text{Cu}_3\text{P}/\text{C}-15\%$ electrode at different scan rates.

Table S1. Specific capacitances of the Cu_3P -based electrodes at different scan rates.

Specific capacitance (C g^{-1})	5 mV s^{-1}	10 mV s^{-1}	20 mV s^{-1}	30 mV s^{-1}	50 mV s^{-1}	80 mV s^{-1}	100 mV s^{-1}
$\text{Cu}_3\text{P}/\text{C}$	353.6	235.3	204.1	191.5	173.6	155.3	131.2
$\text{Cu}_3\text{P}/\text{C}-3\%$ Ni	394.0	267.0	227.7	210.0	188.8	168.0	157.9
$\text{Cu}_3\text{P}/\text{C}-4\%$ Ni	562.6	397.0	320.0	279.5	235.0	200.0	184.9
$\text{Cu}_3\text{P}/\text{C}-5\%$ Ni	694.0	441.4	347.5	303.8	257.5	220.6	204.8
$\text{Cu}_3\text{P}/\text{C}-6\%$ Ni	700.0	561.0	465.0	410.6	346.0	291.9	264.8
$\text{Cu}_3\text{P}/\text{C}-10\%$ Ni	534.0	437.2	368.9	328.6	272.2	215.4	188.0
$\text{Cu}_3\text{P}/\text{C}-15\%$ Ni	382.3	304.0	255.7	231.8	202.5	173.5	158.1

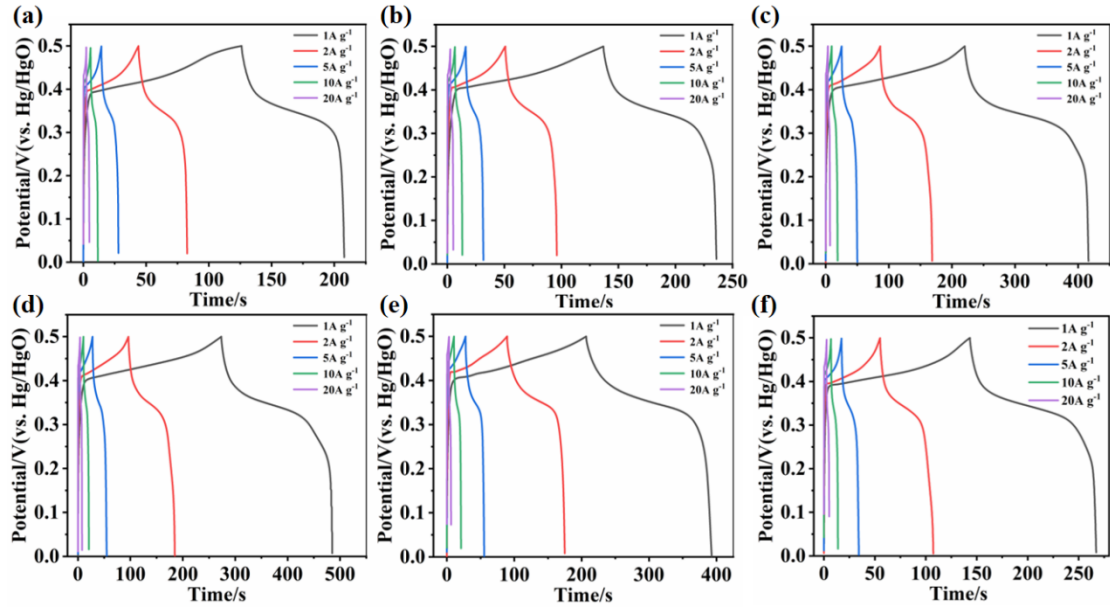


Fig. S11. GCD curves of (a) Cu₃P/C; (b) Cu₃P/C-3% Ni; (c) Cu₃P/C-4%; (d) Cu₃P/C-5%; (e) Cu₃P/C-10% and (f) Cu₃P/C-15% electrode at different current densities.

Table S2. Specific discharge capacitance of Cu₃P-based electrodes.

Specific capacitance (C g ⁻¹)	1 A g ⁻¹	2 A g ⁻¹	5 A g ⁻¹	10 A g ⁻¹	20 A g ⁻¹
Cu ₃ P/C	81.8	77.6	68.5	58	48
Cu ₃ P/C-3% Ni	99.1	90.4	77.5	65	52
Cu ₃ P/C-4% Ni	196	164.8	124.5	94	68
Cu ₃ P/C-5% Ni	211.7	177	135.5	104	78
Cu ₃ P/C-6% Ni	283.8	232.2	173.5	134	98
Cu ₃ P/C-10% Ni	186.2	171	138	105	62
Cu ₃ P/C-15% Ni	123.9	104.8	85	69	52

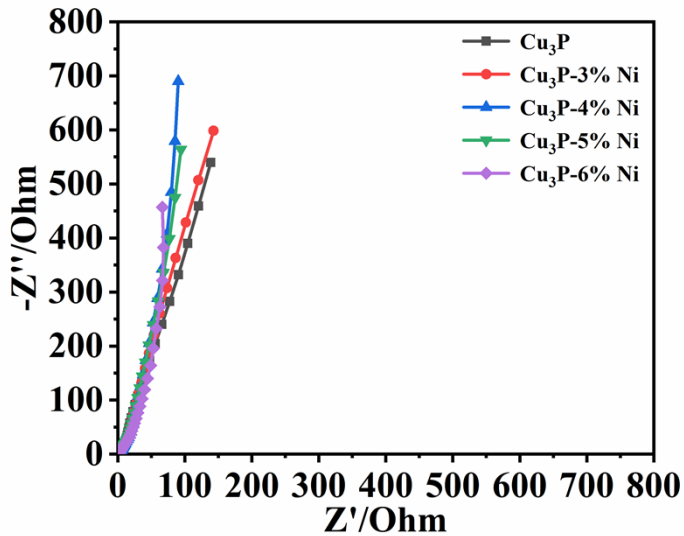


Fig. S12. EIS plots of Cu₃P-based-samples.

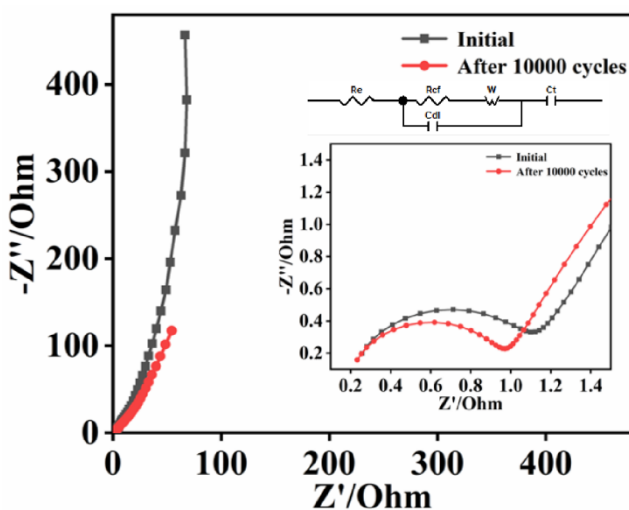


Fig. S13. EIS plots of initial and after 10000 cycles, inset shows the equivalent circuit and enlarged section.

Reference:

- [S1] J. Lin, C. Zeng, X. Lin, C. Xu, C.-Y. Su, CNT-Assembled Octahedron Carbon-Encapsulated Cu₃P/Cu Heterostructure by In Situ MOF-Derived Engineering for Superior Lithium Storage: Investigations by Experimental Implementation and First-Principles Calculation, *Adv. Sci* 7 (2020)